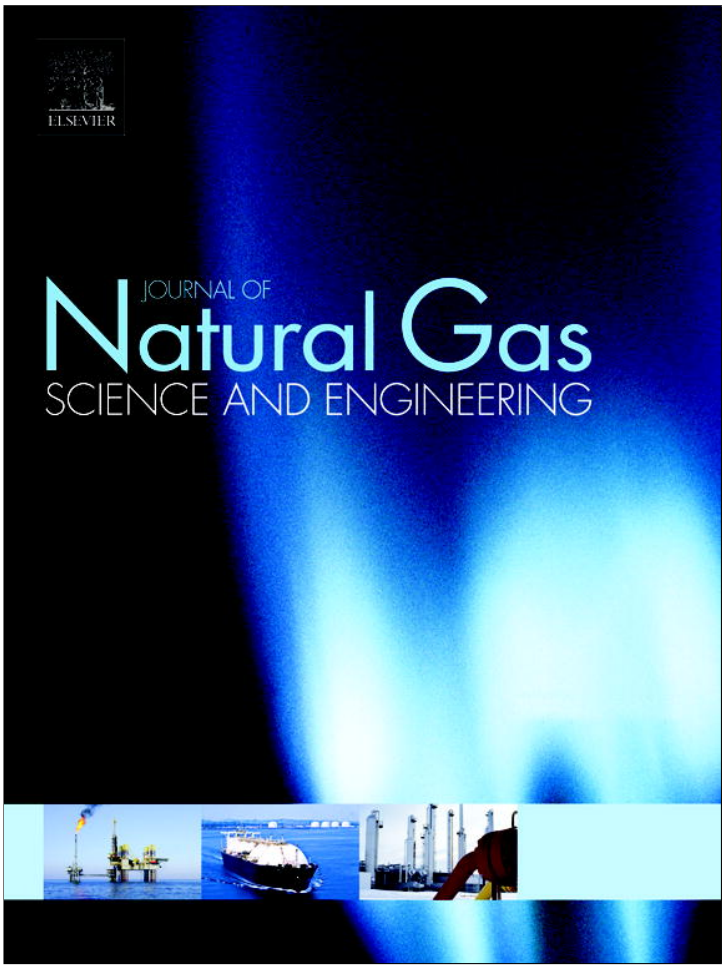

Journal of Natural Gas Science and Engineering 13 (2013) 30–41

Contents lists available at SciVerse ScienceDirect

Journal of Natural Gas Science and Engineering

journal homepage: www.elsevier.com/locate/jngse

Analysis of supersonic separators geometry using generalized radial basis function (GRBF) artificial neural networks

B. Mahmoodzadeh Vaziri, A. Shahsavand*

Department of Chemical Engineering, Faculty of Engineering, Ferdowsi University of Mashhad, Mashhad, Iran

ARTICLE INFO

Article history:
Received 8 November 2012
Received in revised form
10 January 2013
Accepted 10 March 2013
Available online

Keywords:
Supersonic separator
Artificial neural network
GRBF
Design
Trend analysis

ABSTRACT

Supersonic separators (3S) are comprised from unique combination of known physical processes, combining aero-dynamics, thermo-dynamics and fluid-dynamics to produce an innovative gas conditioning process. Condensation and separation at supersonic velocity is the key to achieve a significant reduction in both capital and operating costs. Natural gas dehydration, ethane extraction, LPG production and natural gas sweetening are some potential applications of 3S units among many others. Feed-forward artificial neural networks (ANNs) are also powerful tools for empirical modeling of various engineering processes. Generalized radial basis function (GRBF) networks which are kernel based ANNs, have the best approximation property since they represent the optimal solution of multivariate linear regularization theory. A large set of synthetic data are generated in this work via the fundamental modeling of 3S units and are used to train an optimal GRBF network. The trained network is then used to properly design two pilot and industrial scale 3S units for natural gas dehumidification processes. Furthermore, the trained network is successfully and much more rapidly used for trend analysis purposes to investigate the effect of various input parameters. The conducted research clearly demonstrates the acceptable performance of such neural networks for both design and trend analysis purposes.

1. Introduction

Supersonic separator is a revolutionary device in gas processing industry due to its very small size, low capital and operating costs and superior performance capabilities compared to other conventional equipments. This device is well suited for separating water and liquid hydrocarbons from natural gas streams. As shown in Fig. 1, in a near adiabatic expansion within this device, the gas accelerates to supersonic velocity (Ma ≈ 1.6) and the flow temperature falls considerably ($\Delta t \approx 80\,^{\circ}C$). Such immense temperature drop leads to severe nucleation and condensation of water and heavy hydrocarbons. The swirling effect induced inside 3S unit via plenum chamber produces extremely large centrifugal accelerations (≈300,000–500,000g) and efficiently removes the created water and hydrocarbon droplets. After the liquid collection point, the natural gas pressure can be recovered via different scenarios as received proper attention in our previous work (Ghanbari Mazidi et al., in press). More detailed description of 3S units and their performances are presented elsewhere (Schinkelshoek and Epsom, 2008; Mahmoodzadeh Vaziri et al., 2011). A typical diagram illustrating throat and normal shock wave locations and 3S total length is shown in Fig. 2. As it can be seen, Mach number at throat condition is equal to one and the normal shock wave should happen after collection point. The normal shock wave is crucial for pressure recovery.

Supersonic separators have been received lots of attentions in the recent years due to their numerous advantages such as smaller, lighter, cheaper required instruments, lower installation and handling costs, relatively rapid start-up and less hydrate sedimentation accompanied with fewer environmental emissions compared to conventional separators used oil and gas industries. It is especially well suited for offshore and subsea natural gas separations, due to its lightweight and the viability of unmanned operation (Alfyorov et al., 2005; Betting and Epsom, 2007). Applications of 3S units can lead to huge savings in oil and gas industries because such separators do not require any type of chemical solvents (e.g. tri-ethylene glycol (TEG)), adsorbents (e.g. silica-gel) or other toxic materials.

Considering the above advantages, supersonic separators can be potentially recruited in many chemical and petrochemical engineering processes such as natural gas dehumidification, hydrocarbon dew point control, subsea gas processing, bulk removal of CO_2 and H_2S, ethane recovery, LNG applications, mercury removal, LPG extraction and NGL separation from associated gases

* Corresponding author. Tel.: +98 511 8805124; fax: +98 511 8816840.
E-mail addresses: shahsavand@um.ac.ir, shahsavand@um.ac.ir (A. Shahsavand).

1875-5100/$ – see front matter © 2013 Elsevier B.V. All rights reserved.
http://dx.doi.org/10.1016/j.jngse.2013.03.004

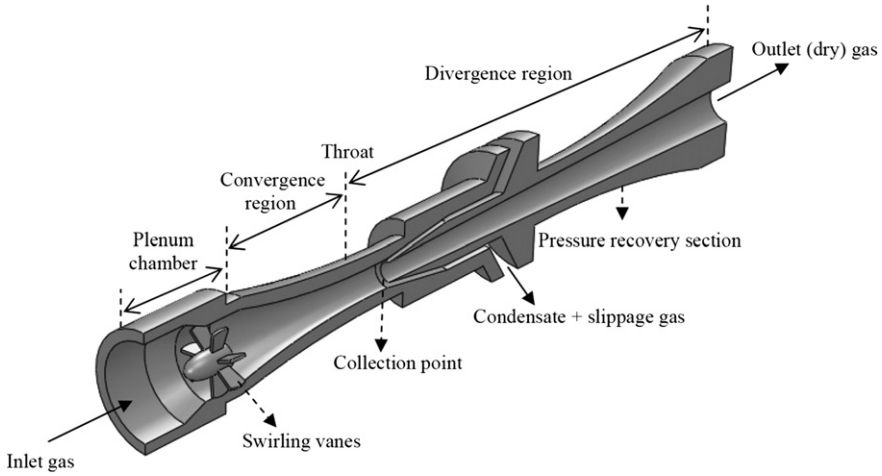

Fig. 1. Typical supersonic separator structure.

(Schinkelshoek and Epsom, 2008; Mahmoodzadeh Vaziri et al., 2011; Alfyorov et al., 2005; Betting and Epsom, 2007).

A detailed literature review on 3S units has been presented in our previous works (Ghanbari Mazidi et al., in press; Mahmoodzadeh Vaziri et al., 2011). In more recent years, several other articles were also published considering various aspects of 3S units.

Jassim et al. (2008) studied the effect of nozzle geometry and vorticity by inserting a constant area channel between the nozzle and diffuser parts of the system. They selected various lengths of such extended constant area regions. Their results emphasized that variation of the channel length would impact the position of the normal shock wave location and the minimum temperature of the system. They also pointed out that gas stream pressure losses are mainly due to inlet swirling flow and vorticity increases very sharply in the vicinity of the normal shock wave. They concluded that "the region just before the shock spot is the main region where fine particles can be separated because of the large vorticity strength".

Ghanbari Mazidi et al. (in press) compared the performances of two supersonic separator structures for the pressure recovery purposes. The first structure contained one nozzle-diffuser where normal shock wave was used for pressure recovery and the second structure consisted of two successive nozzle-diffusers to achieve this purpose. The simulation results clearly showed that both structures behave very similar on pressure recovery, when real gas behavior is assumed and non-isentropic operation was considered.

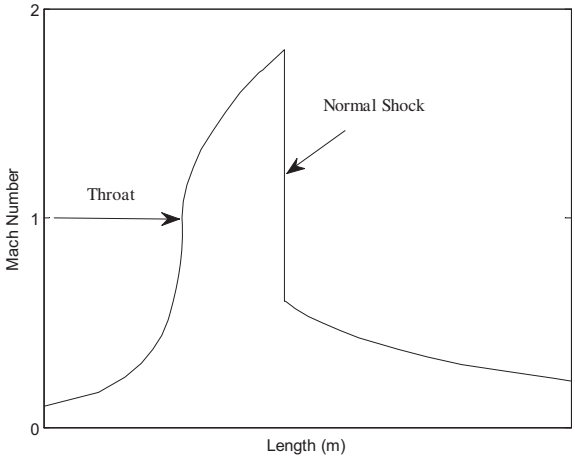

Fig. 2. Typical diagram illustrating throat and shock wave locations and 3S total length.

Karimi and Abdi (2009) investigated the influences of various inlet operating variable (e.g. pressure, temperature and flow rate) and 3S outlet (back) pressure on the overall performance of the 3S unit. They pointed out that shock wave location shifts toward the nozzle outlet when the inlet pressure or back pressure is decreased and the inlet temperature is increased. Malyshkina (2008) and Wen et al. (2011) used computer aided fluid dynamic software to analyze the non-uniform radial distribution of various parameters such as tangential velocity and static temperature. They also mentioned that the non-uniformity of radial distribution of the gas dynamic parameters considerably affects the efficiency of extraction of components. In another article, Malyshkina (2010) presented a method for Primary estimation of the purification efficiency of natural gases in a 3S unit which depended on their entrance conditions of the gas stream. The results showed that the purification efficiency depends on the temperature, pressure, and Mach number of the gas stream during flow inside 3S unit and it is also a strong function of the liquid phase composition of the gas–liquid mixture. The reported results indicate that the amount of liquid formed increases with decreasing temperature and increasing Mach number of the gas stream inside 3S unit. It was preferable to use separators with Mach number values of 1.4–1.8 at liquid collection point.

Wen et al. (2012) studied the particle trajectories and separation efficiency of 3S device by using the Discrete Particle Method (DPM). They used an experimental set up for testing the separation efficiency of three new designed separators with saturated wet air. They mentioned that the separation efficiency reached over 95%, when the length of the cyclone separation section was about 10 times of the throat diameter. Rashidi et al. (2010) presented a rigorous mathematical model combined with the real gas property package to predict the temperature, pressure, velocity and Mach number profiles across the entire 3S unit. An illustrative real case study was also presented to demonstrate the separation mechanism of condensed water and heavy hydrocarbons inside the separator. They showed that more than 84 percent of condensed water and a small fraction of condensed hydrocarbon liquid should be separated from the cooled fluid to meet the pipeline specifications of the natural gas.

Wen Ming et al. (2009) investigated the influences of flow friction drag on spontaneous condensation of water vapor flow inside supersonic Laval nozzles. It was found that the flow friction

has a direct effect on the spontaneous condensation process and therefore it is important to use accurate friction factor predictions when designing this kind of Laval nozzles. A mathematical model for phase equilibrium prediction of multi-component gas separation process inside a supersonic separator was established by Ling Ling et al. (2010). Their model was then used to predict the phase equilibrium characteristics and the separation performance of a field test supersonic separator for purification of a real natural gas flow. Mahmoodzadeh Vaziri et al. (2010) investigated the non-isentropic performance of supersonic separator. The simulation results clearly indicated that the non-isentropic process causes a pre-mature shock occurrence which inhibits sufficient gas cooling and hinders proper liquid separation. They showed that the diverging nozzle angle and inlet gas velocity have an appreciable effect on the pressure recovery ratio of the 3S unit. Furthermore, they pointed out that the non-isentropicity of the process due to form friction of shock wave had a minor effect on prediction of shock wave location compared with the non-isentropicity created from skin friction inside 3S device.

As mentioned above, several articles have been presented on modeling and simulation of 3S processes, all of them based on either complex theoretical models or simulation using computational fluid-dynamics software's that is relatively costly, time-consuming and require high computational capacity. To the best of our knowledge, empirical models such as artificial neural networks (ANNs) have not been used for modeling and simulation of 3S process.

As we know, the geometry of 3S has direct and vital effect on optimal extraction of target components from natural gas stream and the corresponding pressure recovery ratio. Therefore, the present article employs a trained neural network for estimation of optimal 3S geometry (angles and dimensions) in both pilot and industrial scales. The trained ANN may also be used to investigate the effect of various important parameters (such as inlet pressure, temperature, velocity, pressure recovery and outlet velocity) on geometry and dimensions of 3S unit.

2. Artificial neural networks

The 3S process is a nonlinear system of multiple variables, with strong coupling between variables and severe uncertainty. The difficulties presented in using conventional modeling techniques to model such highly nonlinear and complex system with large numbers of inputs and outputs make the application of ANNs to these problems particularly attractive because of their capability for nonlinear mapping and lack of necessity for detailed mechanistic knowledge. ANNs have been widely used in many fields such as process modeling, control, optimization and prediction (Chen and Woodley, 2002; Aminian, 2010).

Radial basis function (RBF) networks, which have solid theoretical foundation based on multivariate regularization theory are extremely powerful feed-forward ANNs. They have been chosen here for predicting the 3S unit behavior over a wide range of operating conditions. Owing to a number of advantages compared with other types of ANNs, such as: robustness, better approximation capability, simpler network structure, short learning time, sensitivity of the model when dealing with noisy data and not getting stuck in local minima (Qu et al., 2009; Ni et al., 2009), RBF networks have found immense applications as a modeling tool in various chemical engineering processes in recent years.

2.1. RBF networks

RBF networks are universal approximators. They can approximate any continuous function and have a very strong mathematical foundation rooted in multivariate regularization theory for solving ill-posed problems (Poggio and Girosi, 1990a,b). The theoretical basis of the feed-forward RBF approach lies in the field of interpolation of multivariate functions (Sarimveis et al., 2004; Tatlier et al., 2005; Kashaninejad et al., 2009).

The typical structure of a RBF network is illustrated in Fig. 3. It consists of three layers, namely the input, hidden and output layers. Each layer consists of a number of neurons (nodes). The nodes in the input layer are used only to pass the input data to the hidden layer. No calculations are performed in the input layer nodes, and the connection between the input and the hidden layer are not weighted.

The hidden layer contains M nodes, which apply a nonlinear transformation on the input variables. A graphical representation of a hidden layer node is depicted in Fig. 4. Each neuron $j = 1, 2, \ldots, M$ in the hidden layer has two sets of parameters namely a center c_j (which lives in the input space dimensions) and width or spread σ_j (a real constant for the isotropic case) associated with it.

For each input vector $X_i = [x_1, x_2, \ldots, x_p]$ and $i = 1, 2, \ldots, p$, the Euclidean norm $\upsilon(\vec{X}_i - \vec{c}_j)$ of the difference between the input vector and the node center is computed as follows:

$$\upsilon_{ij} = \left\|\vec{X} - \vec{c}_j\right\|^2 = \sqrt{\sum_{i=1}^{p} (x_i - c_{j,i})^2} \tag{1}$$

The output of the hidden layer nodes is determined by a nonlinear basis function (also called the "activation function"). The activation function of the hidden neurons $(\phi(\vec{X}))$ is usually radially symmetric in the input space $(\upsilon_{ij} = \upsilon_{ji})$ and the output of each hidden unit depends only on the radial distance between the input vector and the center parameter for that hidden neuron. Some of the common types of RBF are Duchon radial cubic spline, radial quadratic plus cubic and Gaussian function (Aminian, 2010; Srinivasa Pai et al., 2008; Korres et al., 2002). The last one is defined as follows for the case of isotropic spread:

$$\phi_i(\vec{X}) = \exp\left(-\frac{\upsilon^2}{\sigma^2}\right) = \exp\left(-\frac{\left\|\vec{X} - \vec{c}_j\right\|^2}{\sigma^2}\right) \tag{2}$$

In contrast to the sigmoid function, such kernel or basis function is classified as a local activation function. In most of back propagation networks, the argument of the basis function projects the multi-dimensional input space into a scalar one. While, in kernel based RBF networks, the Euclidean norm is used to transform the input vector into a single scalar. A set of synaptic weights is applied to the connection between the hidden and the output layer. The nodes in

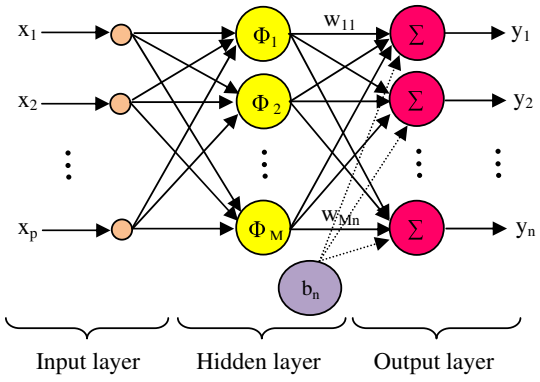

Fig. 3. Schematic of RBF network architecture.

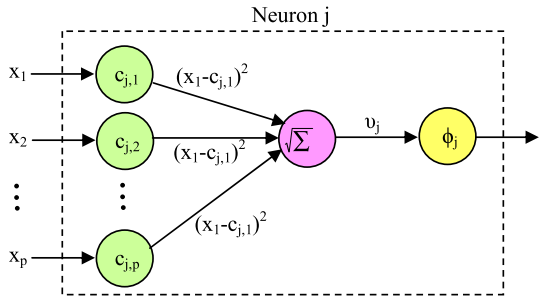

Fig. 4. Schematic of hidden layer neuron.

the output layer serve only as summation units, which produce the final output of the network:

$$y_j(\vec{X}) = \sum_{i=1}^{M} w_{ij}\phi_i(\vec{X}) + b_j; \quad j = 1,\ldots,n \tag{3}$$

where $y_j(\vec{X})$ is the output at the jth node in the output layer, w_{ij} is the weight factor from the ith hidden node to the jth output node and b_j is the bias parameter associated with the jth output node. In fact, the RBF model can be viewed as a sequence of two mappings. The first is a nonlinear mapping of the input data via the basis function and the second is a linear mapping of the basis function outputs via the weights to the network output (Coelho et al., 2009). Therefore, for the given centers and spreads the training of the RBF network reduces to the solution of a linear set of equations to compute the required synaptic weights.

If all training data points are selected as the RBF network centers, then training of the so called "Regularization network" is a trivial task for a given value of isotropic spread. An efficient algorithm was previously developed to find the optimum value of the isotropic spread (Shahsavand, 2009). Such networks can be constructed and trained via the so-called "exact fit" of MATLAB neural network toolbox. In the present work, this type of RBF network could not be practically used from MATLAB toolbox because of the extremely large number of data points involved in the training process.

To relax the one-to-one correspondence between the training exemplars and the RBF network neurons, the so called "Generalized RBF network" of Poggio and Girrosi (1990a,b) or the "fewer neurons" RBF structure of the MATLAB® neural network toolbox (ver. 7.9 (R2009b)) was used in the current work.

2.2. Network architecture

Determining an appropriate architecture of a neural network for a particular problem is an important issue, since the network topology directly affects its computational complexity and its generalization capability. In this study, a novel empirical model based on RBF network is explored to determine the dimension and geometry of 3S in both experimental and industrial scales. Whereas increase in number of neurons did not improve the accuracy (specially systems dealing with many input and output vectors such as 3S system) and to ease the computational load, it is essential to break the one-to-one connection in the conventional RBF network by using a smaller number of neurons, such networks have been labeled as Generalized Radial basis function (GRBF) networks. Consequently, the training of a GRBF network reduces to a challenging large-scale nonlinear optimization problem which has received considerable attention over the past decade.

The network structure that has been used in the current study is illustrated in Fig. 5. It is a two-layered feed-forward GRBF network with multiple inputs and multiple outputs (MIMO). As it is shown in Fig. 5, the inlet pressure (P_i), inlet temperature (T_i), inlet velocity (V_i), inlet flow rate (Q_i), pressure recovery (PR) and outlet velocity (V_e) are the input vectors while the converging section angle (α), diverging section angle (β), throat location (X_{th}), shock wave location (X_{sh}) and the total length of the 3S unit (X_e) are the output parameters of the GRBF network. In any conventional natural gas dehumidification process the dry gas should contain water vapor less than the standard value of 7 lbs water per MMSCF dry natural gas. In all forthcoming simulations, the minimum temperatures occurring in the 3S Laval nozzle, lead to water vapor pressures much lower than the value required to meet the above specification. On the other hand, the 3S unit exit velocity controls the extent of pressure recovery and should be investigated more thoroughly.

As it was mentioned earlier, MATLAB neural network toolbox provides various types of radial basis function networks such as "exact fit design" and "fewer neurons design" for function approximation purposes. The exact fit design uses as many neurons as there are input vectors. The drawback to this design is that it may not return an acceptable solution when many input vectors are needed and over-fitting problem may be occurred in the absence of regularization. Over-fitting can be avoided by resorting to the optimal level of regularization which is embedded in the optimal linear weights of the GRBF network as pointed out by Poggio and Girrosi (1990a,b). Another disadvantage of this design is that it requires more computational space than the fewer design. The more efficient design (fewer neurons) which implemented with "*newrb*" (a new radial basis network) title in MATLAB environment creates a two layer network. The first layer (hidden layer) has "*radbas*" neurons (radial basis neurons), and calculates its weighted inputs with "*dist*" (Euclidean distance weight function, which applies weights to an input to get weighted inputs), and its net input with "*netprod*" (net input function which calculates a layer's net input by combining its weighted inputs and biases). The second layer (output layer) has "*purelin*" neurons (linear transfer function neurons which calculates a layer's output from its net input), calculates its weighted input with "*dotprod*" (dot product weight function) and its net inputs with "*netsum*" (sum net input function). Both layers have their own biases.

Initially the hidden layer has no neurons, and then neurons are added to the hidden layer of a radial basis network until it meets the specified mean squared error (MSE) goal or the maximum number of neurons is reached.

2.3. Data generation and data preprocessing

Since sufficient experimental data on pilot or industrial scale 3S units are not available, hence both training and testing data were generated by a theoretical model presented in our previous works

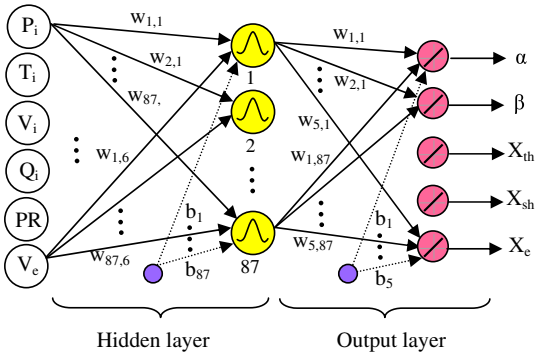

Fig. 5. Network structure applied in the current study.

Table 1
The range of operating condition used in data generation.

Variables	Inlet temp. (K)	Inlet pressure (atm)	Inlet velocity (m/s)	Pressure recovery (%)	Outlet velocity (m/s)	Flow rate (m^3/s)
Range	293–343	7.5–90	15–75	60–90	15–75	0.025–1.85

(Ghanbari Mazidi et al., in press; Mahmoodzadeh Vaziri et al., 2011), in a wide range of operating conditions as shown in Table 1.

Initial data were generated at random on a 6×6817 grid in the input domain and the required outputs were then computed. In the generation phase, five inputs are kept constant while the sixth one varied in the corresponding domain. The number of discretization for each input was selected separately based on the individual characteristic and importance of that input. Peng-Robinson equation of state is used to consider the gas non-idealities. The synthetic data were divided at random into two different training and test (validation) data sets. The training set included 90 percent of the entire data and the test set contained the remaining 10 percent.

When all the input-output variables are of the same order of magnitude, the training algorithm performs better and the forecasting capability can be increased (Sarimveis et al., 2004; Zheng et al., 2011). Otherwise, the entire set of input data should be normalized to a scale of zero to one prior to using them for training or testing processes. Normalization of data may also help to avoid overflows that may appear due to extremely large or very small weights.

2.4. Training the neural network

Network learning is equivalent to finding a surface in a multi-dimensional space that provides the best fit to the training data. The training algorithms tried to find centers and corresponding weights for a particular spread which minimizes MSE (Wang et al., 2006). The training of the network between the inputs and hidden layer occurs in an unsupervised fashion while the training of the network between the hidden and output layers take places in a supervised style based on target outputs.

2.5. Neural network performance

The performance of a GRBF network depends on the number and positions of the radial basis functions, their shape, and the synaptic weights. If they are not appropriately chosen, the RBF network may degrade validity and accuracy of modeling (Coelho et al., 2009).

Initially, the number of the hidden neurons must be selected. This is a key parameter that affects mostly the prediction capabilities of the network. A small number of nodes may result in a network that will not be able to approximate well the original system, while a large network may lead to the over-fitting phenomenon with small recall errors but large generalization deviates. This problem arises specially in the absence of regularization. When the Gaussian function has been selected as the basis function, the isotropic spread should be adjusted to control the amount of overlapping of adjacent neurons.

In this article, different numbers of hidden layer neurons and various values of isotropic spreads are considered. Fig. 6 shows the plots of norm (mean of squares) of recall and generalization errors with respect to number of neurons and isotropic spread.

As shown in Fig. 6, the optimal number of hidden layer neurons and the corresponding optimal spread values were selected via minimization of mean of squared error (MSE) in a trial–error approach as 87 and 0.55, respectively.

In the absence of optimal level of regularization, the value of MSE usually decreases monotonically with increasing the number of hidden layer neurons, because more neurons provides much larger degrees of freedom and forces the model to pass through each and every training data. Using optimal level of regularization (coupled with selection of optimal spread) restricts the degrees of freedom and may increase the MSE value when the number of hidden layer neurons exceeds the optimal value.

Various centers selection techniques, such as K-means clustering, linear regression, C-means clustering and Kohonen algorithms may be used. In each of these techniques, the parameters of the basis functions are determined through the unsupervised or supervised training algorithms. Various means clustering algorithms look for convenient clusters of data and place the RBF centers in the middle of each cluster (Aminian, 2010). In the present study the K-means clustering algorithm locates the center vector and the orthogonal least squares (OLS) algorithm calculates the optimal weight values.

Figs. 7 and 8 present the recall and validation performances[1] of neural network for prediction of throat and shock wave locations, 3S total length and also converging and diverging angles. As you can see, the model could not pass through all training data because of lack sufficient degrees of freedom. Evidently too much flexibility (excessive degrees of freedom) may lead to over-fitting phenomenon which is not desirable. Tables 2 and 3 provide the statistical analysis of the GRBF network for both recall and validation performances.

As it can be seen, all validation (generalization) performances provide relatively acceptable trends for predicting the above strategic points of 3S units. In the next section, the optimal geometries and dimensions of 3S processes in both pilot and industrial scales will be estimated by using the above trained GRBF network. The main advantage of using trained optimal network instead of conventional theoretical simulations is its quicker response. Once a GRBF network is trained, the prediction of the geometry and all other parameters can be performed very quickly. While, the theoretical approach requires much longer times to achieve the same objective.

3. Prediction of 3S optimal geometry via trained GRBF

The performance of supersonic separator and its separation efficiency are very sensitive to scale and geometry of this device, hence proper selection of correct geometry can ameliorate effectiveness of 3S units in both pilot and industrial operations.

3.1. Typical pilot unit specifications

In a typical design (for our in-house laboratory scale scheme), dry natural gas (methane) is assumed to flow into 3S unit at a temperature of around 20 °C, a pressure of 7.5 atmospheres, a actual volumetric flow rate (at operating temperature and pressure) of 0.025 m^3/s which is equivalent to about 21,000 SCMD and an inlet velocity of about 22 m/s. For practical reasons the 3S unit

[1] Recall performance provides the predictions of the trained network, while validation performances illustrate the trained network predictions.

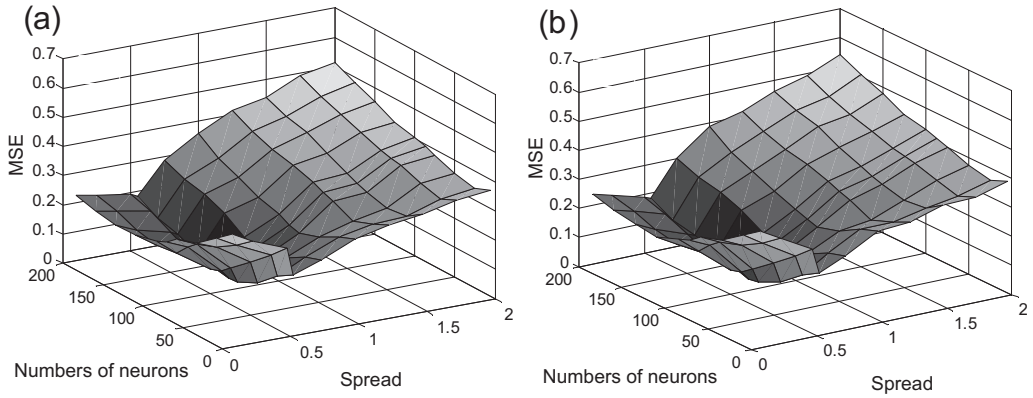

Fig. 6. Profile of spread values and number of hidden layer neurons versus MSE: (a) for recall performance, (b) for validation performance.

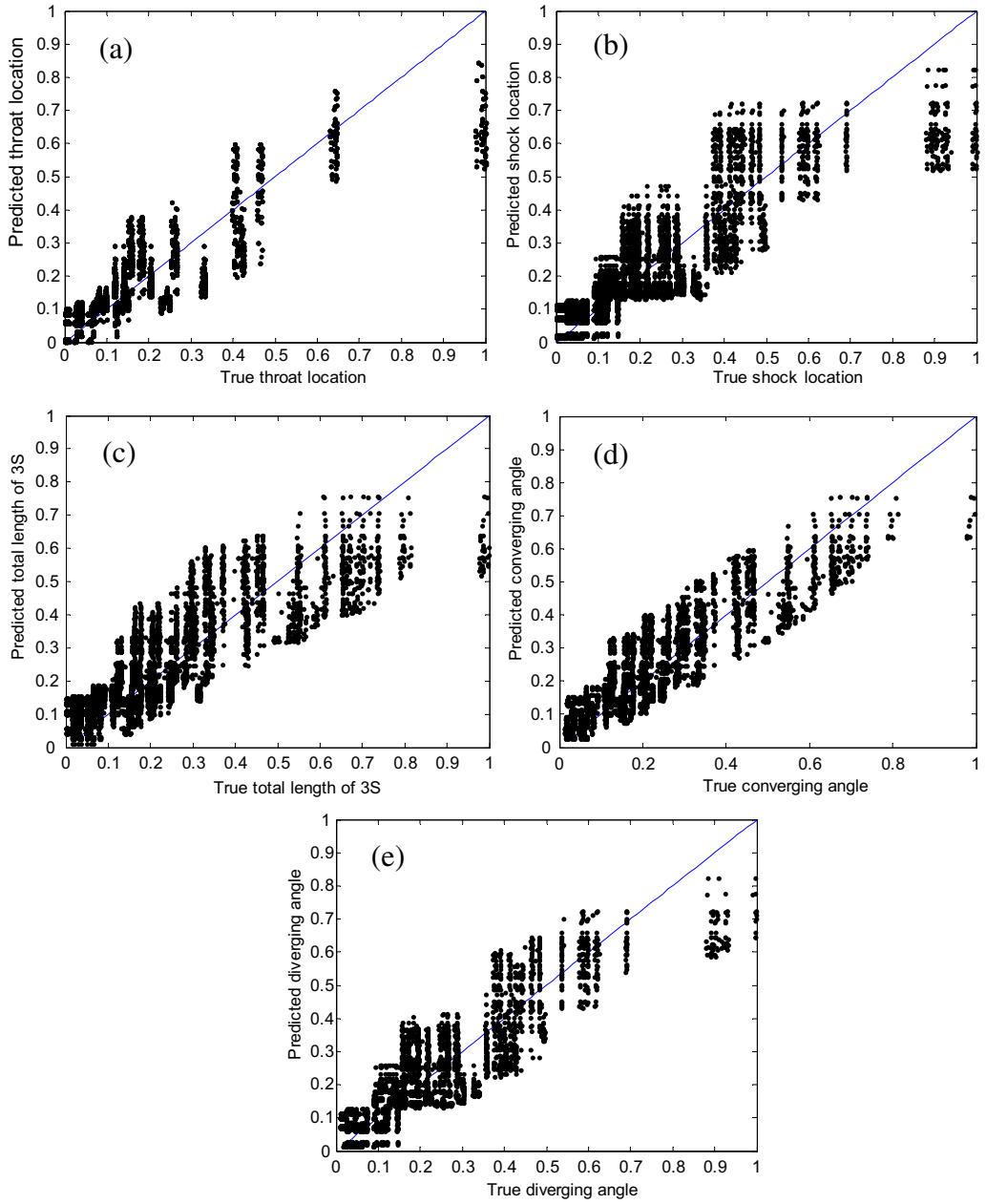

Fig. 7. Recall performances of GRBF for prediction of: (a) throat, (b) shock wave locations, (c) entire length of 3S, (d) converging angle and (e) diverging angle.

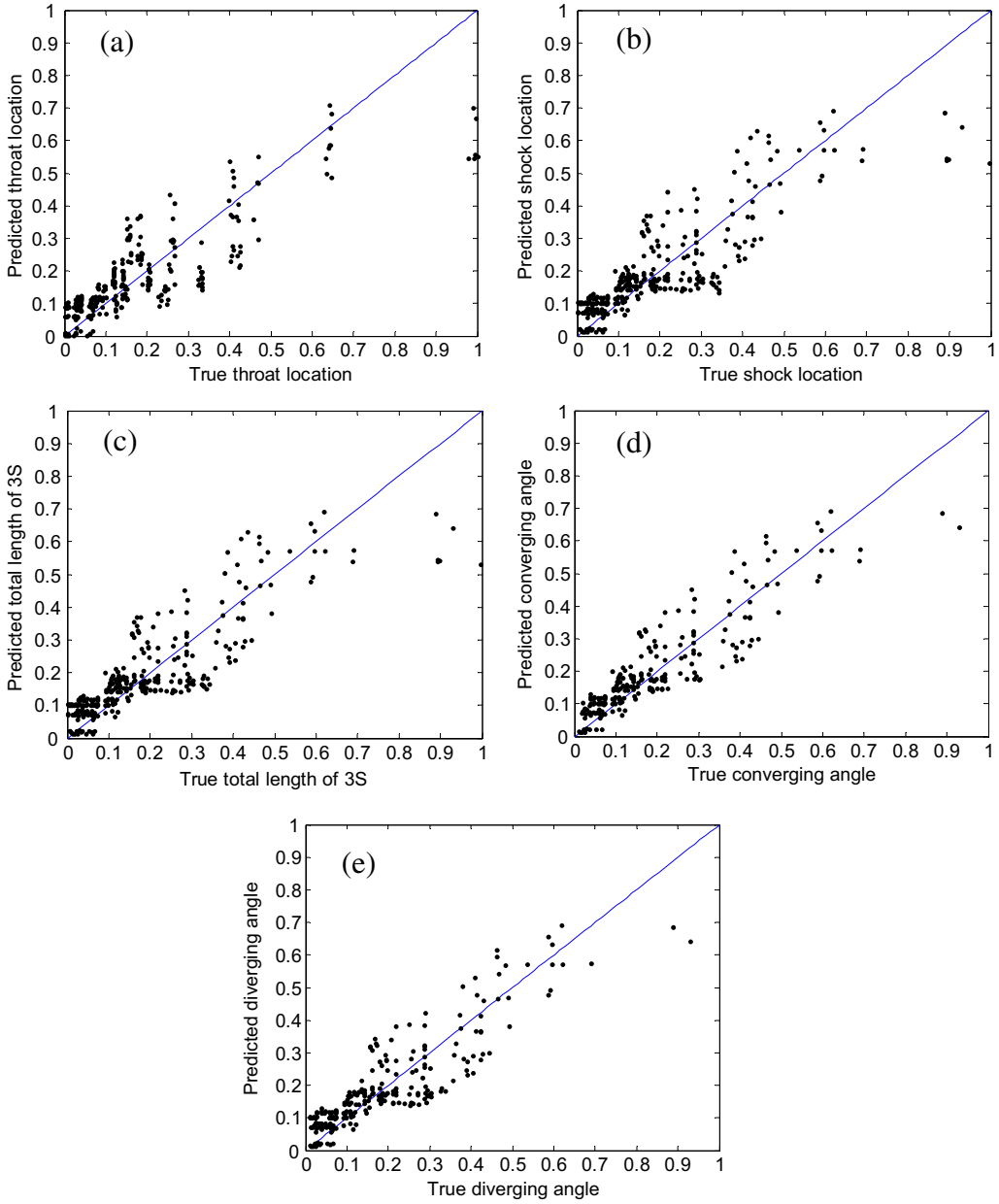

Fig. 8. Validation performances of GRBF for prediction of: (a) throat, (b) shock wave locations, (c) entire length of 3S, (d) converging angle and (e) diverging angle.

Table 2
Statistical analysis of the GRBF network recall performances.

	X_{th}		X_{sh}		X_e		α		β	
	Pr	Tr	Pr	Tr	Pr	Tr	Pr	Tr	Pr	Tr
Average	0.305	0.304	0.314	0.313	0.333	0.332	0.367	0.365	0.344	0.343
Minimum	0.0004	0	0.0036	0	0.0047	0	0.007	0	0.0036	0
Maximum	0.862	1	0.838	1	0.776	1	0.783	1	0.831	1
SD	0.176	0.219	0.169	0.208	0.153	0.206	0.151	0.202	0.167	0.206
CV	0.577	0.721	0.538	0.664	0.459	0.621	0.411	0.553	0.485	0.601
MSE	0.0031	0.0048	0.0028	0.0043	0.0023	0.0042	0.0025	0.0046	0.0024	0.0047
R	0.911		0.921		0.905		0.901		0.924	
Intercept	0.0726		0.0725		0.1023		0.1002		0.0709	
Slope	0.853		0.847		0.841		0.862		0.859	

SD, Standard deviation; CV, coefficient of variation; MSE, mean squared error; R, correlation coefficient; Pr, predicted values by GRBF network; Tr, true values obtained by theoretical model.

Table 3
Statistical analysis of the GRBF network validation performances.

	X_{th}		X_{sh}		X_e		α		β	
	Pr	Tr	Pr	Tr	Pr	Tr	Pr	Tr	Pr	Tr
Average	0.203	0.205	0.212	0.213	0.232	0.229	0.236	0.231	0.224	0.226
Minimum	0.0006	0	0.0054	0.0003	0.0086	0.0001	0.0091	0.0002	0.0058	0.0004
Maximum	0.736	1	0.705	0.996	0.706	0.994	0.704	0.989	0.703	0.993
SD	0.169	0.22	0.163	0.206	0.15	0.198	0.148	0.194	0.159	0.201
CV	0.833	1.072	0.766	0.967	0.646	0.864	0.627	0.839	0.709	0.889
MSE	0.0028	0.0048	0.0026	0.0042	0.0022	0.0039	0.0022	0.0039	0.0026	0.0042
R	0.905		0.908		0.906		0.906		0.909	
Intercept	0.0824		0.0815		0.1045		0.1045		0.0815	
Slope	0.851		0.845		0.837		0.867		0.861	

SD, Standard deviation; CV, coefficient of variation; MSE, mean squared error; *R*, correlation coefficient; Pr, predicted values by GRBF network; Tr, true values obtained by theoretical model.

outlet velocity is assumed to be the same as its inlet velocity. Test unit was taken into account for 75 percent pressure recovery. The predictions of GRBF network and the computed results of our previous theoretical model are presented in Table 4. As it can be seen, the optimally trained RBF network (using optimal number neurons and optimum isotropic spread) is perfectly capable to predict 3S dimension and its corresponding geometries.

The next section compares similar performance of GRBF networks for an existing industrial gas treating unit.

3.2. Prediction of optimal 3S unit for dehumidification of Khangiran refinery sweet gas

Around 10 MMSCMD (1.845 m^3/s at 7237.5 kPa (1050 psia) and 55 °C) sweet natural gas containing around 98.5% methane enters each of four dehumidification units of Khangiran refinery (located in north-east of Iran). After dehumidification by silica-gel bed, the gas is injected into two 36-inches pipelines with a pressure of around 61.22 atm (6203 kPa or 900 psia). For practical reasons, the pressure recovery of this unit should be at least 86 percent ($6203 \times 100/7237.5$) to meet the pressure demand of the 36 inches pipelines.

The gas velocity in inlet pipeline to GTU plant is about 9 m/s, which is very low and it is not proper for entering the 3S unit; because small swirling will be created at this low gas velocity. Therefore, the pipe diameter of 3S plenum chamber is assumed to be reduced to 8 inches which produces relatively higher velocity of about 57 m/s. Note again that, the outlet velocity of 3S unit was considered to be equal to the inlet velocity of entering gas at all cases. The predictions of the GRBF network for the above conditions of sweet gas leaving GTU plant and entering 3S unit are presented in Table 5. The obtained results of theoretical model are also included. As been clear, the constructed network can extremely well predict the 3S unit geometrical features for an industrial scale process.

In the light of the above comparisons for both pilot and industrial scales case studies, we may conclude that supersonic separators are much more suitable for comparison of various industrial scale designs at high gas flow rates. As it can be seen in the above examples, when the gas flow rate increases as much as 70 times, the length of 3S unit only increases around 7 times. In other words, the 3S unit geometry stays relatively small for very large flow rates.

Table 4
Comparison of GRBF network results with theoretical model predictions for a pilot scale 3S unit.

Geometry & Dimension	Unit	GRBF network	Theoretical model	Relative error (%)
Converging angle (α)	deg	13.4	12.9	3.87
Diverging angle (β)	deg	7.6	7.2	5.55
Throat location (X_{th})	m	0.067	0.064	4.68
Shock wave location (X_{sh})	m	0.075	0.072	4.16
Total 3S length (X_e)	m	0.113	0.108	4.62
Inlet diameter (D_i)	m	0.038	0.038	0
Throat diameter (D_{th})[a]	m	0.0061	0.008	23.75
Shock location diameter (D_{sh})[b]	m	0.0082	0.010	18
Outlet diameter (D_e)[c]	m	0.0384	0.038	1.05

[a] Throat diameter was computed from $D_{th} = D_i - 2X_{th}\tan(\alpha)$.
[b] Shock wave location diameter was computed from $D_{sh} = D_{th} + 2(X_{sh} - X_{th})\tan(\beta)$.
[c] Outlet diameter was computed from $D_e = D_{sh} + 2(X_e - X_{sh})\tan(\beta)$.

4. Trend analysis via optimally trained GRBF network

Previously constructed and trained GRBF neural network for simulation of Khangiran natural gas refinery dehumidification units is used to investigate the effects of various operating parameters on the overall geometry of 3S unit. In each case, all base parameters are kept constant and only input variable under consideration (inlet pressure, inlet temperature, inlet velocity, pressure recovery and outlet velocity) is changed and its effect on the desired output (converging angle, diverging angle, throat location, throat diameter (D_{th}), normal shock location, normal shock diameter (D_{sh}), outlet diameter (D_e) and total length of 3S unit) is investigated.

4.1. Effect of inlet pressure

Fig. 9 illustrates the effect of inlet pressure on various 3S unit dimension and geometry for real gas flow. As it can be seen, distinctive optimal points can be detected for nearly all

Table 5
Comparison between results of GRBF network and robust mathematical model for 3S dimensions and geometries of Khangiran refinery dehumidification units.

Geometry & Dimension	Unit	GRBF network	Theoretical model	Relative error (%)
Converging angle (α)	degrees	13.42	13.98	4.00
Diverging angle (β)	degrees	7.45	7.02	6.12
Throat location (X_{th})	m	0.202	0.21	3.80
Shock wave location (X_{sh})	m	0.305	0.29	5.17
Total 3S length (X_e)	m	0.795	0.768	3.51
Inlet diameter (D_i)	m	0.203	0.203	0
Throat diameter (D_{th})	m	0.106	0.099	7.07
Shock location diameter (D_{sh})	m	0.133	0.119	11.76
Outlet diameter (D_e)	m	0.341	0.308	10.71

Various diameters of 3S unit are computed as mentioned earlier in Table 2.

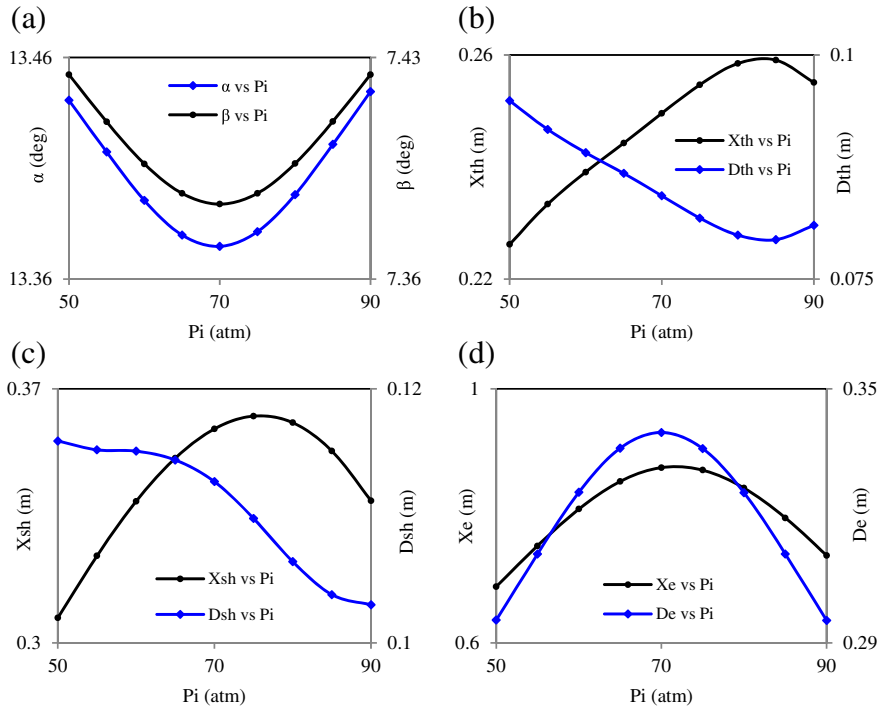

Fig. 9. Effect of inlet gas pressure on various 3S dimensions and geometries: (a) Converging and diverging angles, (b) throat location and diameter, (c) normal shock location and diameter, (d) total length and outlet diameter.

geometrical dimensions. For example, the inlet pressure of around 70 atm. leads to minimum converging and diverging angles, outlet diameter and 3S unit total length. Some of these optimal points cannot be simply explained due to the complexity of the incompressible processes. On the other hand, much higher pressures are required to attain maximum throat lengths because of decrease in entering gas velocity at higher inlet pressures. The decrease in throat location with increase in high inlet pressures

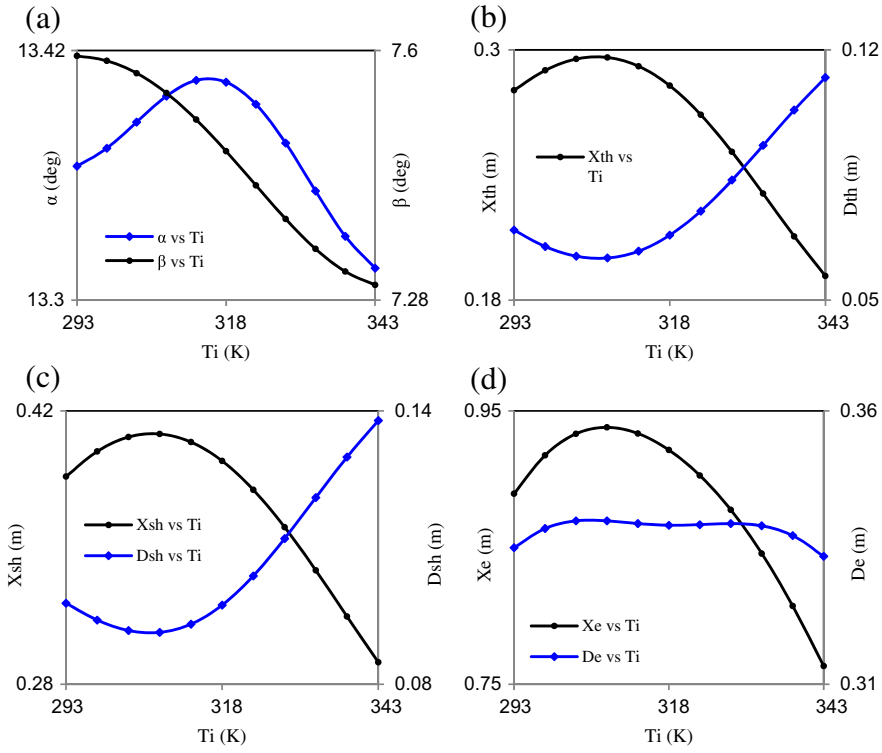

Fig. 10. Effect of inlet gas temperature on various 3S dimensions and geometries: (a) converging and diverging angles (b) throat location and diameter (c) normal shock location and diameter (d) total length and outlet diameter

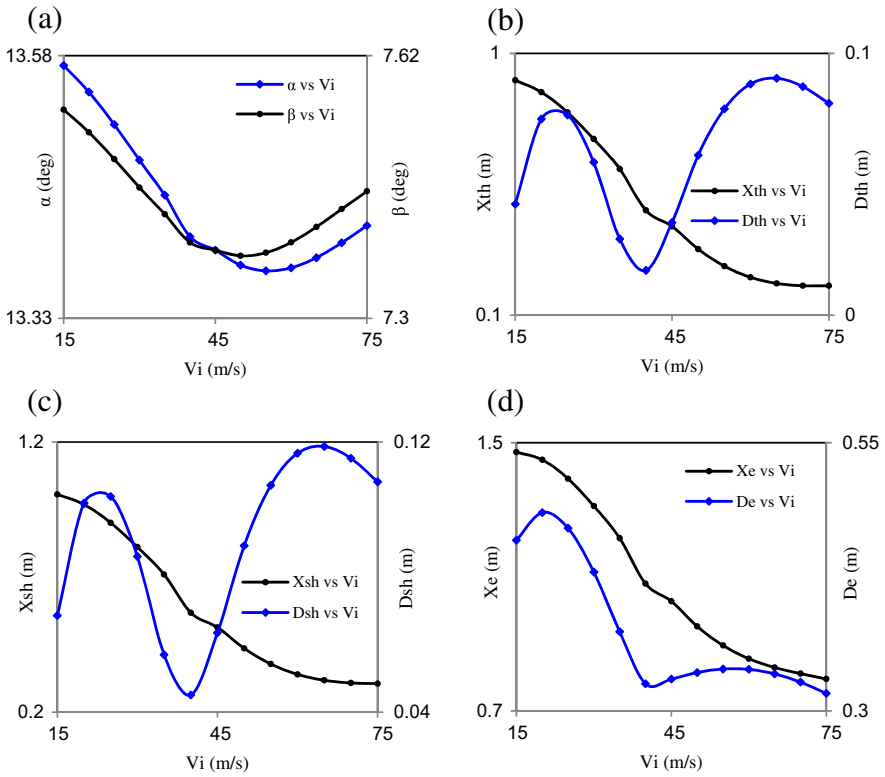

Fig. 11. Effect of inlet gas velocity on various 3S dimensions and geometries: (a) Converging and diverging angles, (b) throat location and diameter, (c) normal shock location and diameter, (d) total length and outlet diameter.

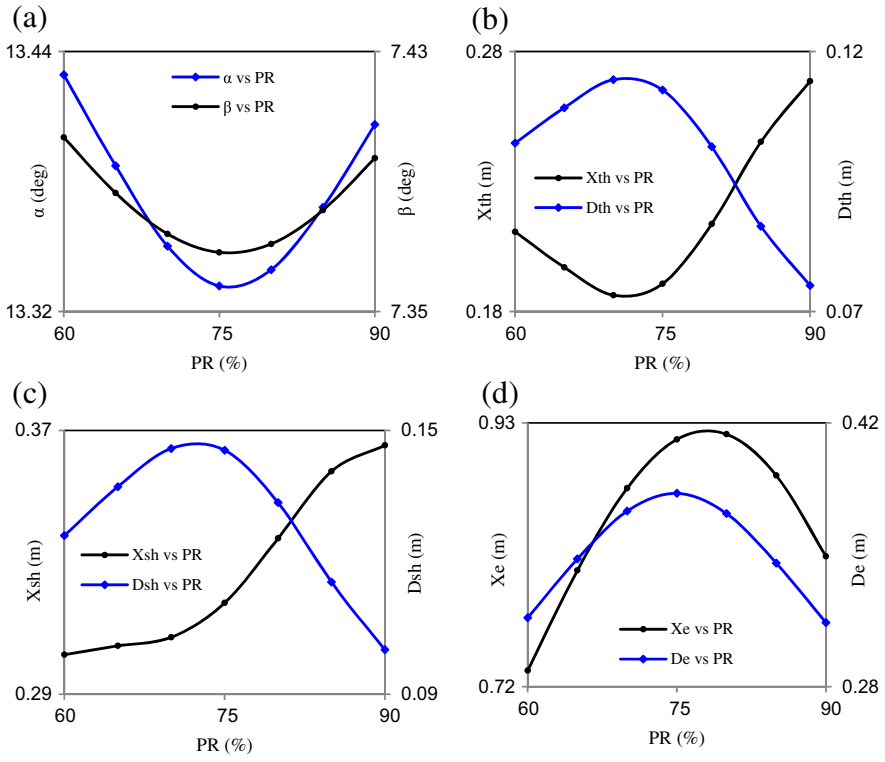

Fig. 12. Effect of pressure recovery on various 3S dimensions and geometries: (a) converging and diverging angles, (b) throat location and diameter (c) normal shock location and diameter (d) total length and outlet diameter.

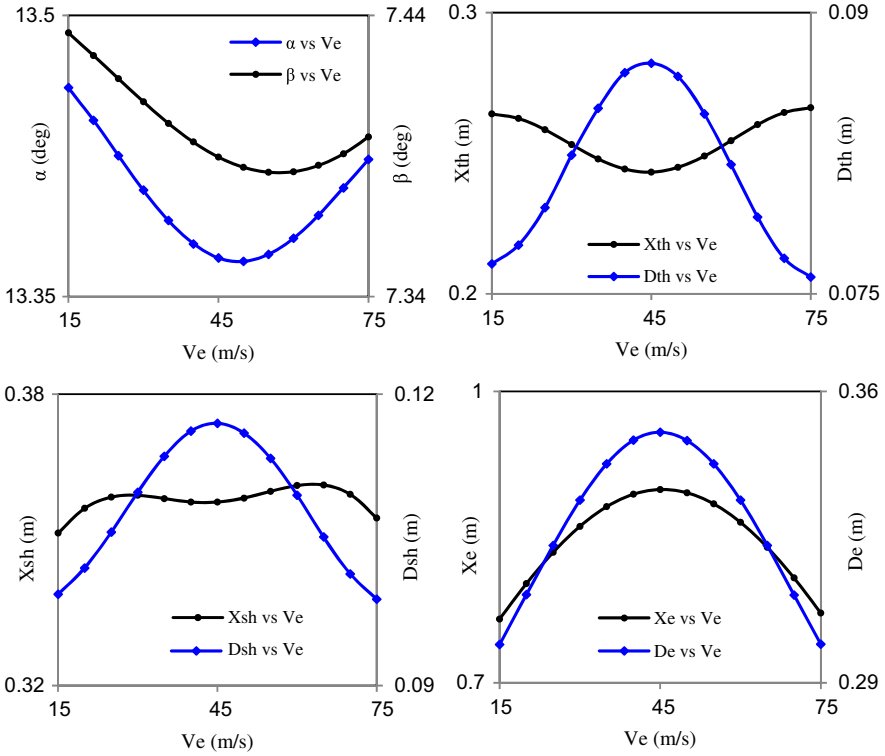

Fig. 13. Effect of outlet velocity on various 3S dimensions and geometries: Top left: converging and diverging angles. Top right: throat location and diameter. Bottom left: normal shock location and diameter Bottom right: total length and outlet diameter.

may be due to non-ideality of the gas behavior. Evidently, the shock wave location follows the same trend because the throat location plays a major role on this issue. The total length of the 3S unit will eventually reduces with increase in inlet pressure because of the small distances required between shock wave location and outlet condition for these situations.

4.2. Effect of inlet temperature

Fig. 10 illustrates the effect of inlet gas temperature on 3S unit dimensions and corresponding geometries. Similar discussion as presented in previous section applies here. As can be shown, diverging angle of 3S unit slightly decreases with increasing inlet temperature although converging angle has a pick value at 313 K. Throat location, shock location and total length of 3S include increasing-decreasing trend with rising inlet temperature, while throat and shock diameters have a reverse trend. Also, outlet diameter is almost constant with variation of inlet temperature. Note that, the normal shock location is constant relative to the total length of 3S unit.

4.3. Effect of inlet velocity

In Fig. 11, the inlet velocity effect of real gas flow on 3S dimension and geometry are presented. As shown, converging and diverging nozzle angles are reduced with increasing inlet gas velocity to 50 m/s and then increases. Obviously, the throat location, shock location and total length of 3S unit are decreased when the inlet gas velocity increases. This is due to requiring less distance to attain sonic velocity. On the other hand, throat diameter, shock location diameter and outlet diameter periodically change with increase in inlet gas velocity.

4.4. Effect of pressure recovery

The pressure recovery effects of real gas flow on 3S dimensions and geometries are shown in Fig. 12. As illustrated, the minimum value of converging and diverging nozzle angles occur around 75 pressure recovery percent. Throat location shows distinctive minima while normal shock location shifts toward 3S outlet when pressure recovery increases. Surprisingly, as shown in Fig. 12, the total length of 3S reduces in higher pressure recovery (up to 80 percent). On the other hand, pressure recovery rising to about 70–75 percent provides maximum diameters of strategic parts of 3S unit (throat, normal shock and outlet).

4.5. Effect of outlet velocity

In Fig. 13, the outlet velocity effect of real gas flow on various 3S dimensions and geometries are presented. As can be seen, the lowest values of converging and diverging angles occur in the range of 50–55 m/s of outlet velocity. Unlike other previously mentioned parameters, the outlet velocity does not have any significant effect on the throat and shock locations. Furthermore, the outlet velocity of 45 m/s provides maximum values for total length of 3S unit and the diameter of key points (throat, normal shock and outlet).

5. Conclusions

Artificial neural networks are powerful empirical methods for multidimensional hyper-surface reconstruction. They can be successfully used for modeling of 3S complex process which incorporates multiple parameters and variables. This procedure has a simple topological structure that avoids lengthy or very time-

consuming calculations. It was clearly shown that a certain type of neural network (GRBF) can successfully predict the dimensions and geometries of supersonic separator in various scales over wide ranges of operating conditions.

The main advantage of using trained optimal network instead of conventional theoretical simulations is its quicker response. Once a GRBF network is properly trained, the prediction of the geometry and all other parameters for design purposes can be performed very quickly and efficiently. While, the theoretical approach requires much longer computation times to achieve the same task. The trained neural network with optimal parameters (linear weights, isotropic spread and number of neurons) can also be adequately used for trend analysis purposes.

Nomenclature

Symbols

b	bias parameter associated with the output node
c	center of the hidden layer neuron
D_e	outlet diameter of the supersonic separator (m)
D_i	inlet diameter of the supersonic separator (m)
D_{sh}	normal shock wave diameter in the supersonic separator (m)
D_{th}	throat diameter of the supersonic separator (m)
M	number of neurons in the hidden layer of the GRBF network
n	number of neurons in the output layer of the GRBF network
p	number of neurons in the input layer of the GRBF network
P_i	inlet gas pressure to the 3S unit (atm)
PR	pressure recovery percent (%)
Q_i	inlet gas flow rate to the 3S unit (m^3/s)
T_i	inlet gas temperature to the 3S unit (K)
V_e	outlet gas velocity from the 3S unit (m/s)
V_i	inlet gas velocity to the 3S unit (m/s)
w	weight factor from the hidden node to the output node
x	input variable in the GRBF network
X	input vector in the GRBF network
X_e	total length of the 3S unit (m)
X_{sh}	shock wave location in the supersonic separator (m)
X_{th}	throat location in the supersonic separator (m)
y	network response

Greek letters

α	converging section angle of the supersonic separator (degree)
β	diverging section angle of the supersonic separator (degree)
υ	Euclidean norm of the difference between the input vector and the node center
Φ	activation function of the hidden neurons of the GRBF network
σ	width or spread of hidden layer neuron

Subscripts

i	counter of input variable number in the input layer of the GRBF network
j	counter of neuron number in the hidden layer or outputs of GRBF network

References

Alfyorov, V., Bagirov, L., Dmitriev, L., Feygin, V., Imayev, S., Lacey, J., 2005. Oil and Gas Journal, 53–58.

Aminian, A., 2010. Chemical Engineering Journal 162, 552–556.

Betting, M., Epsom, H., 2007. World Oil Mag 228, 197–200.

Chen, B.H., Woodley, J.M., 2002. Computers & Chemical Engineering 26, 1611–1620.

Coelho, L.d.S., Freire, R.Z., dos Santos, G.H., Mendes, N., 2009. International Communications in Heat and Mass Transfer 36, 304–313.

Ghanbari Mazidi, M., Shahsavand, A., Mahmoodzadeh Vaziri, B., Petroleum Science and Technology., in press.

Jassim, E., Abedinzadegan Abdi, M., Muzychka, Y., 2008. Petroleum Science and Technology 26, 1773–1785.

Karimi, A., Abdi, M.A., 2009. Chemical Engineering and Processing 48, 560–568.

Kashaninejad, M., Dehghani, A.A., Kashiri, M., 2009. Journal of Food Engineering 91, 602–607.

Korres, D.M., Anastopoulos, G., Lois, E., Alexandridis, A., Sarimveis, H., Bafas, G., 2002. Fuel 81, 1243–1250.

Ling Ling, B., Zhong Liang, L., Heng Wei, L., Wen Ming, J., Ming, Z.H., Jian, Z.H., 2010. Science China Technological Sciences 53, 435–443.

Mahmoodzadeh Vaziri, B., Shahsavand, A., Rashidi, H.R., Ghanbari Mazidi, M., 2010. Proceedings of 13th Iranian National Chemical Engineering Congress and 1st International Regional Chemical and Petroleum Engineering Congress, Razi University, Kermanshah, Iran, October, 2010.

Mahmoodzadeh Vaziri, B., Shahsavand, A., Rashidi, H.R., 2011. Proceedings of 3rd International Congress on Green Process Engineering, Kuala-Lumpur, Malaysia, Dec 6–8, 2011

Malyshkina, M.M., 2008. High Temperature 46 (1), 69–76.

Malyshkina, M.M., 2010. High Temperature 48 (2), 244–250.

Ni, Y., Xiao, W., Kokot, S., 2009. Journal of Hazardous Materials 168, 1239–1245.

Poggio, T., Girosi, F., 1990a. Proceedings of the IEEE 78, 1481–1497.

Poggio, T., Girosi, F., 1990b. Science 247, 978–982.

Qu, N., Mi, H., Wang, B., Ren, Y., 2009. Journal of the Taiwan Institute of Chemical Engineers 40, 162–167.

Rashidi, H.R., Shahsavand, A., Sheibani, V., Mahmoodzadeh Vaziri, B., 2010. Proceeding of second conference on science and engineering of separation, Kerman University, Iran.

Sarimveis, H., Alexandridis, A., Mazarakis, S., Bafas, G., 2004. Computers & Chemical Engineering 28, 209–217.

Schinkelshoek, P., Epsom, H., 2008. GPA 87th Annual Convention, Grapevine, TX, USA, March, 2008.

Shahsavand, A., 2009. Scientia Iranica 16, 41–53.

Srinivasa Pai, P., Mathew, M.T., Stack, M.M., Rocha, L.A., 2008. Tribology International 41, 672–681.

Tatlier, M., Cigizoglu, H.K., Erdem-Senatalar, A., 2005. Computers & Chemical Engineering 30, 137–146.

Wang, L., Shao, C., Wang, H., Wu, H., 2006. Journal of Natural Gas Chemistry 15, 230–234.

Wen, C., Cao, X., Yang, Y., 2011. Chemical Engineering and Processing: Process Intensification 50, 644–649.

Wen, C., Cao, X., Yang, Y., Zhang, J., 2012. Advanced Powder Technology 23, 228–233.

Wen Ming, J., Zhong Liang, L., Heng Wei, L., Hui Zhong, P., Ling Ling, B., 2009. Science China Series E-Technological Sciences 52 (9), 2653–2659.

Zheng, H., Zhu, G., Jiang, S., Tshukudu, T., Xiang, X., Zhang, P., He, Q., 2011. Desalination 269, 148–156.